ACS APPLIED MATERIALS & INTERFACES

Research Article

www.acsami.org

HF-Free Synthesis of Anatase TiO_2 Nanosheets with Largely Exposed and Clean {001} facets and Their Enhanced Rate Performance As Anodes of Lithium-Ion Battery

Xun-Liang Cheng,[†] Ming Hu,[†] Rong Huang,[‡] and Ji-Sen Jiang*,[†]

[†]Department of Physics, Center for Functional Nanomaterials and Devices, and [‡]School of Information Science & Technology, East China Normal University, Shanghai 200241, P.R. China

Supporting Information

ABSTRACT: An interface between toluene and water was utilized to synthesize ca. 10 nm thick of anatase TiO_2 nanosheets (NSs) with 82% exposure of {001} facets. In this procedure, highly corrosive and toxic HF, which was generally used to prepare TiO_2 NSs with largely exposed high energy facets, was avoided. Furthermore, the surfaces of the NSs were quite clean as suggested by XPS analysis. Serving as anode materials in lithium-ion batteries, these as-prepared anatase TiO_2 NSs manifested a low initial irreversible capacity loss (12.5% at 1 *C*), an excellent capacity retention at 10 C charge−discharge rate (101.9 mA h g^{-1} after 100 cycles), and enhanced rate performance at 0.5−10 *C* current rates in compared with Degussa P25 TiO_2 nanoparticles (NPs). Their excellent electrochemical performances were mainly derived from the large proportion of {001} exposed facets and a very short diffusion pathway, which allowed fast and efficient Li^+ transportation in the electrodes.

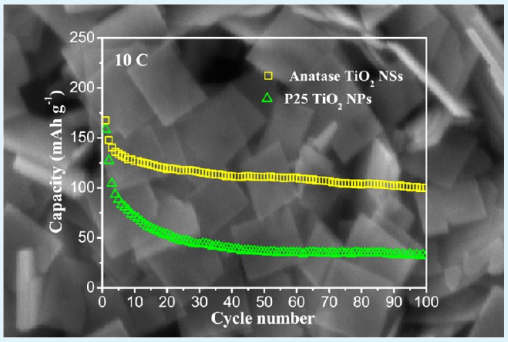

KEYWORDS: *liquid−liquid interface, anatase TiO_2, ultrathin nanosheets, {001} facet, lithium-ion batteries*

1. INTRODUCTION

For its great application potential in photocatalysis, lithium-ion batteries, solar cells, and sensors, titanium dioxide (TiO_2) has been intensively investigated in recent decades.[1] Not only the crystal phases, particle sizes, mesoporous structures but also the exposed facets of TiO_2 can significantly affect their unique physical and chemical properties.[2−5] Accordingly, ultrathin single-crystalline anatase TiO_2 sheets with large proportion of clean high-energy {001} facets have inspired great research interests in recent years.[6,7] It has been theoretically and experimentally demonstrated that the anatase TiO_2 with exposed {001} facets were especially reactive[8] and have shown surface enhanced performance in wide applications such as, photocatalytic degradation of pollutants,[9,10] photocatalytic water splitting[11,12] and dye-sensitized solar cell.[13] This unique nanostructure was found to be quite useful in lithium-ion battery as well. Lou and Yang et al. proved that the ultrathin TiO_2 NSs dominated with {001} facets used as lithium-ion battery anode materials could manifest a much lower initial irreversible capacity loss, higher storage capabilities, and remarkable capacity retention at high current rates compared to TiO_2 nanocrystals with dominantly exposed {101} facets and other anatase TiO_2 nanostructures.[14−16] According to some theoretical studies, the Li^+ ions in anatase TiO_2 diffuse along a zigzag pathway in the *c*-direction (i.e., [001] direction) with the octahedral vacancy sites connected, where the Li^+ ions coordinate with 6 O atoms.[17,18] Theoretical calculations also showed that the energy barriers for Li^+ ions insertion into anatase (001) and (101) surfaces were 1.33 and 2.73 eV, respectively.[15] Such result indicated that Li^+ ions transport much faster across the {001} facets rather than the {101} facets.[15] The enhanced electrochemical properties of the anatase TiO_2 NSs could be attributed to the large proportion of {001} exposed facets which favors Li^+ ions insertion by providing more accessible sites, and the ultrathin plane allows fast and efficient lithium diffusion. Thus, controlled synthesis of ultrathin anatase TiO_2 NSs with highly exposed {001} facets are greatly desirable for high-performance lithium-ion batteries and some other potential applications.

Currently, most synthetic methods rely on the selective adsorption of HF or organic molecules on the {001} facets during the crystal growth.[6] Because the surface free energies of anatase TiO_2 are in the orders of 0.90 J/m^2 for {001}, >0.53 J/m^2 for {100}, >0.44 J/m^2 for {101},[19] most of the available anatase TiO_2 crystals are found in a truncated bipyramidal shape which comprises the thermodynamically stable {101} facets (up to 94%) and a small part of {001} facets to reduce the total surface free energy.[6,7] Since Yang et al. first synthesized micrometer-sized anatase TiO_2 single crystal containing 47% of {001} facets by using HF as a shape

Received: August 3, 2014
Accepted: October 8, 2014
Published: October 8, 2014

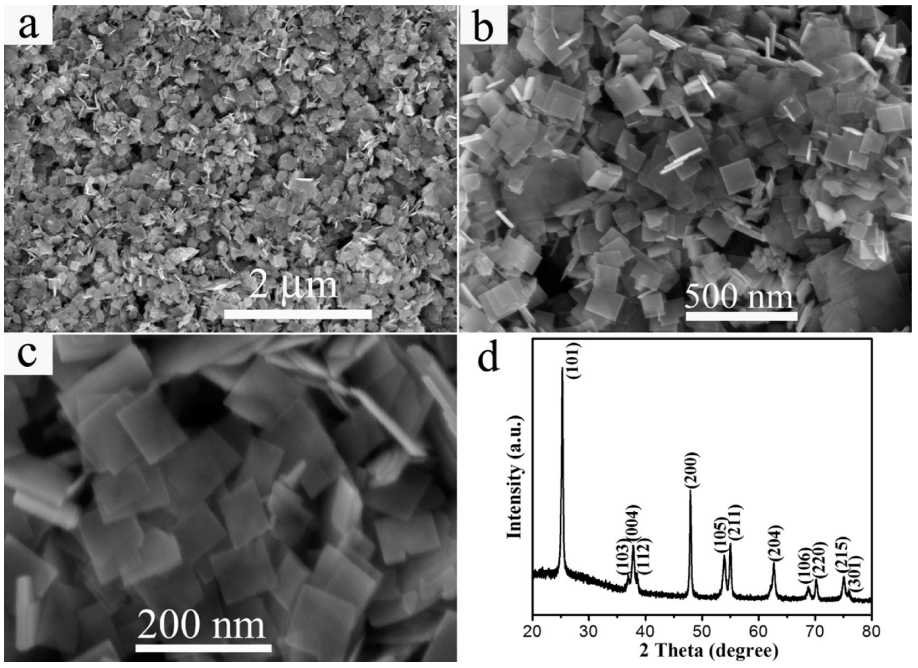

Figure 1. (a–c) Typical FESEM images of the obtained anatase TiO_2 NSs formed at the toluene-water interface. (d) Its corresponding XRD pattern.

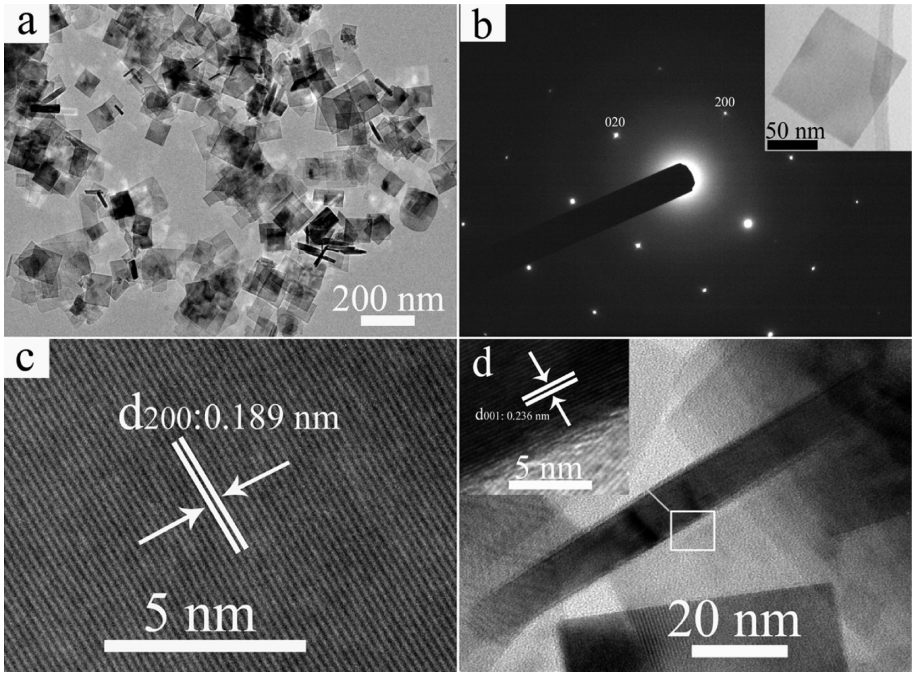

Figure 2. (a) Low-magnification TEM image of the obtained anatase TiO_2 NSs. (b) SAED pattern, and (c) corresponding HRTEM image of a single anatase TiO_2 nanosheet (the inset in b) recorded from the flat square surface. (d) Vertical-view TEM image of an individual TiO_2 nanosheet and its corresponding HRTEM image (inset) recorded from the selected area marked with a white rectangle.

controlling agent,[20] great efforts have been focused on developing synthesis strategies to increase the proportion of the {001} exposed facets and reduce the thickness in the [001] direction. To date, highly corrosive and toxic HF was still the most widely used {001} facets stabilizing agent,[10,20−24] especially for preparing ultrathin anatase TiO_2 NSs dominated with {001} facets.[9,14,15] Stucky and co-workers reported that {001} facets dominated anatase TiO_2 NSs with thicknesses lower than 1 nm can be prepared by a simple nonaqueous way,[25] however, these ultrathin TiO_2 NSs were stabilized by surfactant like oleylamine (~43 wt %) and stacked together. When the surfactant was removed by calcination, the condensation and structure destruction ensue and irregular TiO_2 crystals were produced. Although {001} facets exposed anatase TiO_2 single crystals have also been synthesized by other HF-free synthetic strategies,[11,26−29] such as solvothermal alcoholysis of TiF_4, gas-phase thermal oxidation of $TiCl_4$ or using tetrafluoroborate-based ionic liquid as stabilizing agent, these methods usually produce TiO_2 NSs with limited {001} exposed facets or having large thickness in the [001] direction.

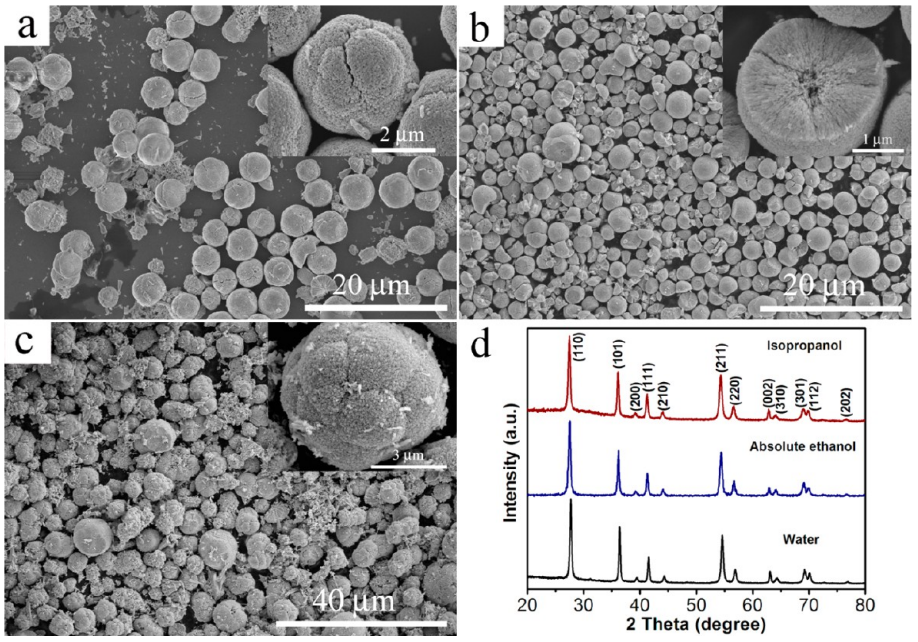

Figure 3. FESEM images of the products synthesized in a mixture of (a) 0.6 mL of TBT, 19.4 mL of isopropanol, 1 mL of water, and 9 mL of hydrochloric acid; (b) 0.6 mL of TBT, 19.4 mL of anhydrous ethanol, 1 mL of water, and 9 mL of hydrochloric acid; (c) 0.6 mL of TBT, 20.4 mL of water, and 9 mL of hydrochloric acid at 180 °C for 24 h. (d) Their corresponding XRD patterns.

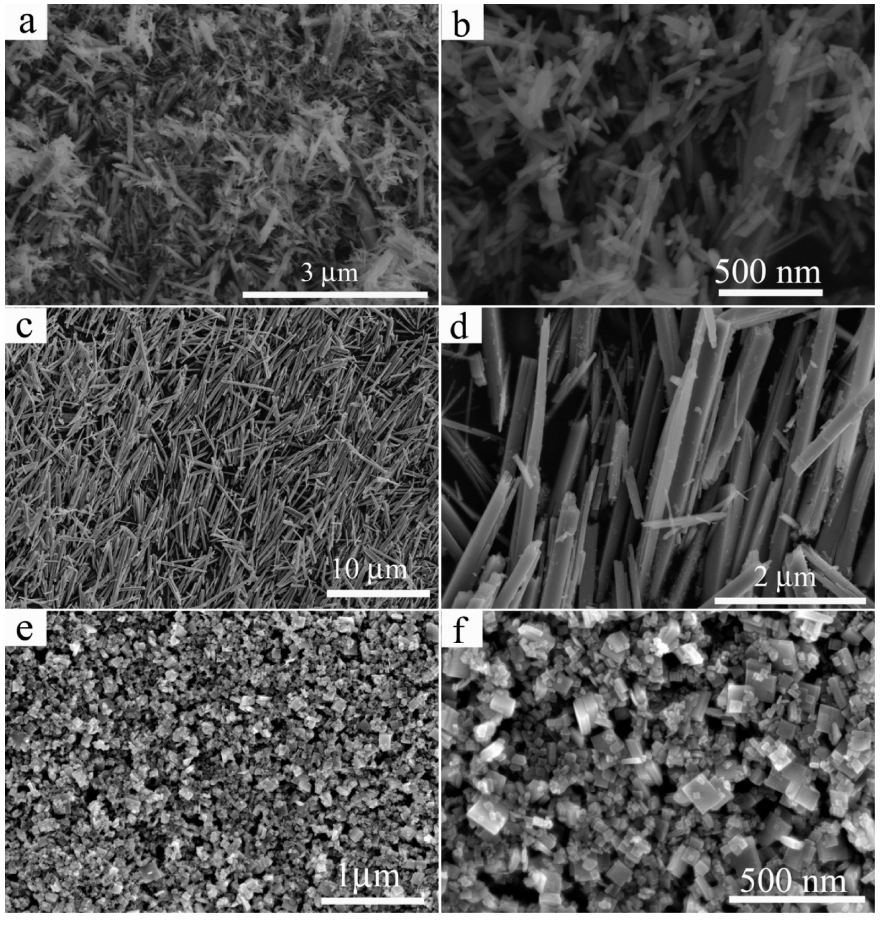

Figure 4. FESEM images of the products prepared with different volume ratios of hydrochloric acid and water: (a, b) 5:5, (c, d) 8:2, and (e, f) 8.5:1.5.

Preparing anatase TiO_2 NSs with high proportion of {001} facets and ultrathin feature with exemption from HF or surfactants is still challenging, because HF is highly corrosive and hazardous. Moreover, HF and surfactants are strongly

adsorbed on the surface of TiO_2 leading to polluted surface of TiO_2. In this work, a unique space, the interface between two immiscible solvents, is utilized to confine the growth of TiO_2, leading to large quantities of ultrathin and {001} facet-dominated anatase TiO_2 NSs. Inspired by the ultrathin feature and large proportion of {001} facets of these anatase TiO_2 NSs, their lithium storage properties were also investigated.

2. EXPERIMENTAL SECTION

2.1. Synthesis of Anatase TiO_2 NSs. Typically, 9 mL of concentrated hydrochloric acid (HCl, 36.5−38 wt %) was diluted with 1 mL of water which was then transferred to a 45 mL Teflon-lined stainless steel autoclave. Subsequently, 20 mL of toluene (hexane or cyclohexane) solution containing 0.6 mL of titanium n-butoxide [$Ti(OC_4H_9)_4$, TBT] was layered on top of aqueous solution without stirring. The autoclave was heated at 180 °C for 24 h followed by cooling to room temperature. Then, the produced off-white powder was collected by centrifugation, followed by washing with ethanol and water for several times and drying at 40 °C for 10 h in air.

2.2. Characterization. The structure and morphology of the products were characterized by field-emission scanning electron microscopy (FESEM; Hitachi S-4800), transmission electron microscopy (TEM; 200 kV, JEOL JEM-2010F) and selected area electron diffraction (SAED; JEOL JEM-2010F). The crystal structure was examined by the X-ray diffraction (XRD; X'Pert-Pro MPD diffractometer) with Cu Kα radiation and conventional θ-2θ geometry. X-ray photoelectron spectroscopy (XPS) was conducted on a RBD upgraded PHI-5000C ESCA system (PerkinElmer) with Mg Kα radiation ($h\nu$ = 1253.6 eV). Binding energies were calibrated by the containment carbon (C 1s = 284.6 eV).

2.3. Electrochemical Tests. The slurry was prepared by mixing 70 wt % of active materials (anatase TiO_2 NSs), 20 wt % of conductivity agent (carbon black, Super P−Li), with 10 wt % of binder (polyvinylidene difluoride, PVDF) in *N*-methyl pyrrolidone (NMP), which was then coated on a copper foil and dried at 80 °C for 12 h in vacuum. The 14 nm electrode was coupled with lithium foil in a CR2032 coin cells in an Ar-filled glovebox (MB-10-compact, MBRAUN) with oxygen and water of less than 0.5 ppm. Celgard 2320 membrane was used as separator. The electrolyte contained 1 M $LiPF_6$ in a mixture of ethylene carbonate (EC) and diethyl carbonate (DEC) (1:1 w/w). Galvanostatic charge−discharge cycles were performed on a LAND CT2001A battery test system within the voltage window of 1.0−3.0 V. Cyclic voltammetry (CV) was carried out on an electrochemical workstation (CHI 660C) between 1.0 and 3.0 V at a scan rate of 0.2 mV s^{-1}.

3. RESULTS AND DISCUSSION

Figure 1a shows the panoramic FESEM image of the nanosized NSs prepared with toluene as organic phase. The magnified FESEM image in Figure 1b reveals these obtained anatase TiO_2 NSs having a well-defined square outline. The magnified FESEM observation in Figure 1c indicates the surfaces of these anatase TiO_2 NSs are quite flat and smooth. The average side length of these anatase TiO_2 NSs is ~92 nm with a thickness of ~10 nm (see statistical data results in Figure S1 in the Supporting Information). Figure 1d exhibits a typical XRD pattern of the obtained TiO_2 NSs, which is conformable to the standard pattern of anatase phase (tetragonal, space group I41/amd, JCPDS No. 21−1272).

In line with the observation in FESEM images, the TEM image shown in Figure 2a further confirms the square geometry structure of the obtained anatase TiO_2 NSs. The selected-area electron diffraction (SAED) pattern (Figure 2b) of the flat square surface of a single nanosheet (insert in Figure 2b) can be indexed into the [001] zone,[10,20] indicating the top and bottom square surfaces are {001} facets. The lattice spacing shown in high-magnification TEM (HRTEM) (Figure 2c) is 0.189 nm, suggesting the (200) planes of anatase TiO_2 single crystals. Figure 2d exhibits a TEM image of a vertical TiO_2 nanosheet, which was magnified in the inset HRTEM image. A lattice spacing of 0.236 nm for the adjacent lattice planes corresponds to the (001) plane of anatase TiO_2.[9,30] In addition, side view for an individual TiO_2 nanosheet (see Figure S2 in the Supporting Information) clearly indicates the side face is not a rectangle but comprised two isoscele trapezoidal surfaces. On the basis of the structural characterization and many recently reported related sheet-like structure,[9,10,20,26] the schematic illustration of the prepared anatase TiO_2 nanosheet was presented in Figure S3 (Supporting Information), in which two square surfaces represent {001} facets and the eight isosceles trapezoidal surfaces indicate the {101} facets. Deduced from the angle between neighboring {001} and {101} facets (68.3°) and the degree of truncation (0.96),[6,10,20,26] the exposed {001} facets accounted for ~82% in the obtained TiO_2 NSs prepared with toluene as organic phase.

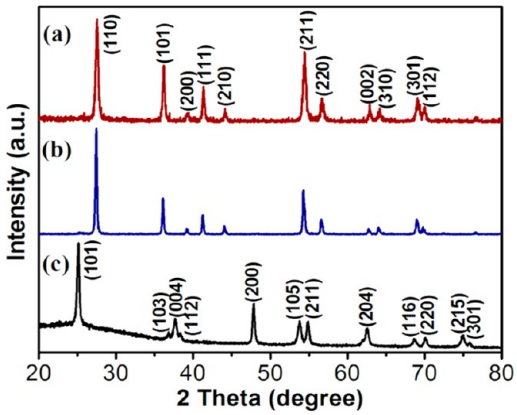

Figure 5. XRD patterns of the products prepared with different volume ratios of hydrochloric acid and water: (a) 5:5, (b) 8:2, and (c) 8.5:1.5.

X-ray photoelectron spectroscopy (XPS) provides information on the surface of the prepared anatase TiO_2 NSs, where characteristic peaks of Ti and O were distinctly observed (see Figure S4a in the Supporting Information). The Ti 2p spectrum shows peaks at 458.7 and 464.4 eV corresponding to the $2p_{3/2}$ and $2p_{1/2}$ spin−orbital components, respectively, suggesting the same oxidation state of Ti in NSs compared to bulk TiO_2 (see Figure S4b in the Supporting Information).[20,31] The binding energy of O 1s at 529.7 eV is attributed to the O_2^- in TiO_2 and O 1s at 532.5 eV is assigned to adsorbed water on the TiO_2 surface (see Figure S4c in the Supporting Information).[20,31,32] No binding energy signals of Cl 2p at around 198.1 and 199.8 eV were recorded (see Figure S 4d in the Supporting Information),[31] suggesting a clean surfaces of the TiO_2 NSs, which is different from the anatase TiO_2 NSs obtained from HF or surfactants.

The two-phase interface plays an important role during the formation of the anatase TiO_2 NSs, which is elucidated through a series of control experiments. In the first control experiment, we respectively used hexane and cyclohexane to replace toluene as organic phase at the same condition. It was found that the products also consisted of numerous square-shaped NSs (see Figure S5 in the Supporting Information). The XRD patterns in Figure S6 (Supporting Information) clearly indicate the TiO_2 prepared with hexane or cyclohexane as organic phase are pure

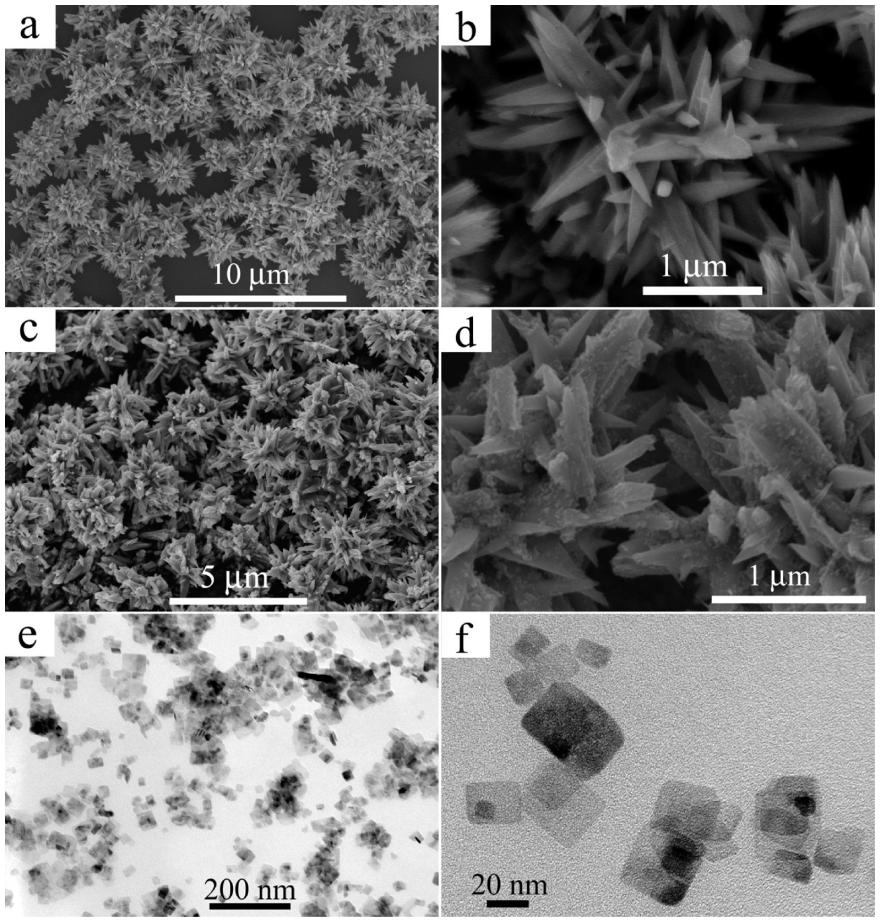

Figure 6. Low-, and high-magnification FESEM images of the products synthesized at 180 °C for (a, b) 2 and (c, d) 3 h. (e, f) Low- and high-magnification TEM images of the products synthesized at 180 °C for 5 h.

anatase (PDF No. 21−1272). In the second control experiment, 0.6 mL of TBT was dissolved in 10 mL of solution containing 9 mL of hydrochloric acid and 1 mL of water, and then 19.4 mL of toluene was added to keep the total reaction solutions volume at 30 mL. After hydrothermal at 180 °C for 24 h, it was found that the solution remained clear and no TiO_2 product formed. In the third control experiment, we used equal volumes of isopropanol, absolute ethanol, and water to replace toluene phase. The reactions were took place in the whole solution since the solvents are miscible with each other. As shown in Figure 3a, the product prepared with 19.4 mL of isopropanol instead of toluene has a 3D spherical microstructure and is composed of numerous nanorods. Similarly, microspheres consisting of densely packed nanorods were formed when using absolute ethanol and water instead of the toluene phase (Figure 3b,c). Their corresponding XRD patterns are presented in Figure 3d, and the obtained products are all pure rutile TiO_2 phase (JCPDS No. 21−1276). These results highlighted the importance of two-phase interface on the formation of anatase TiO_2 NSs.

To unveil the function of HCl in producing the {001} facets exposed anatase TiO_2 NSs, two control experiments were carried out. In the first control experiment, the HCl concentration was changed by tuning volume ratios of hydrochloric acid to water while keeping the total volume at 10 mL. Provided that the volume ratio of HCl and H_2O was balanced at 5:5, the products were composed of many nanorods with different sizes (Figure 4a,b). Increasing the volume ratio of hydrochloric acid to water to 8:2 resulted in the formation of large quantities of TiO_2 microprisms, as shown in Figure 4c and d. When slightly increased the volume ratio of hydrochloric acid to water to 8.5:1.5, many NSs with a wide size distribution formed (Figure 4e, f). The corresponding XRD patterns shown in Figure 5 indicate the products obtained with the volume ratios of hydrochloric acid to water at 5:5 and 8:2 were pure rutile phase (JCPDS No. 21−1276), whereas a higher volume ratio of hydrochloric acid to water at 8.5:1.5 engendered pure anatase (JCPDS No. 21−1272). In the second control experiment, HCl solution was replaced by H_2SO_4 solution while keeping H^+ concentration constant. It was found that the product was composed of small-sized nanoparticles (see Figure S7a in the Supporting Information). The XRD pattern shown in Figure S7b (Supporting Information) confirms their compositions were pure anatase phase of TiO_2 (JCPDS No. 21−1272).

To trace the formation process of the anatase TiO_2 NSs, we collected the products at early stage and investigated by FESEM and TEM (Figure 6). After reacting for 2 h, interestingly, 3D sisal-like TiO_2 microstructures were obtained (Figure 6a). Figure 6b clearly indicates that the sisal-like structure consisted of many interlaced nanopyramids with sharp tips. When reacting for 3 h, the products still kept sisal-like microstructure (Figure 6c). Further examination from the high-magnification FESEM image (Figure 6d) shows that many tiny TiO_2 nanocrystals were formed and scattered on the nanopyramid surfaces. Further increased the reaction time to 5

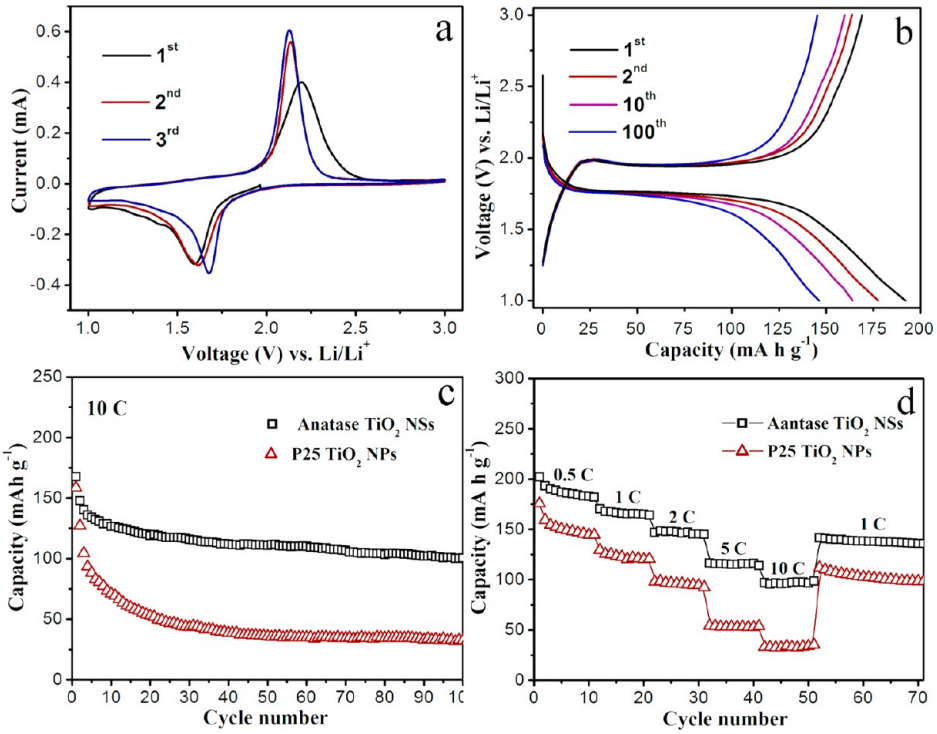

Figure 7. Electrochemical properties of the synthesized anatase TiO_2 NSs. (a) Representative cyclic voltammograms (CVs) at 0.2 mV s^{-1} for the first 3 cycles. (b) Charge−discharge voltage profiles at 1 *C* (170 mA g^{-1}) for the 1st, 2nd, 10th, and 100th cycles. (c) Cycling performances of the anatase TiO_2 NSs and P25 TiO_2 NPs at 10 *C*. (d) Rate capability of the anatase TiO_2 NSs and P25 TiO_2 NPs at 0.5−10 *C*. All of the measurements were conducted at 1.0−3.0 V voltage window.

h, the sisal-like TiO_2 microstructures and small-sized nanocrystals disappeared and rectangular NSs with ca. 15−40 nm in width were produced (Figure 6e, f). The corresponding XRD patterns (see Figure S8 in the Supporting Information) indicate the products prepared for 2 and 3 h were a anatase and rutile mixed-phase and for 5 h was a pure anatase TiO_2 phase.

In view of the above experimental results, the formation of {001} facets exposed anatase TiO_2 NSs might be attributed to an HCl-assisted interfacial growth process. First of all, the selective adsorption mechanism can be ruled out by the clean surface as well as the weak affinity of HCl toward {001} facets.[31] Second, the thickness of the anatase TiO_2 NSs is quite thin which matches with the space between two immiscible solvents. Therefore, the interface between two immiscible solvents is probably the template for the generation of anatase TiO_2 NSs. The key step to make sure the interface can be used as template should be positioning the nucleate and subsequent crystallization process only at the interface. HCl probably plays critical role here. As we can see that the generation of TiO_2 in our case is actually a dissolution-recrystallization process. The dissolved Ti^{4+} ions can coordinate with Cl^- ions to generate complex. It is well-known that $TiCl_4$ is highly affiliate to nonpolar solvent, thus the recrystallization process mainly happens at the interface. When H_2SO_4 was used, no such kind complex formed, and the recrystallization process took place in the whole water phase. On this account, the interface cannot affect the growth of TiO_2 in the absence of HCl. Therefore, the interface here plays as template, whereas the HCl helps to position the reaction inside the interface.

Electrochemical tests were conducted to examine the lithium storage capability of these anatase TiO_2 NSs with 82% of {001} facets. The electrochemical Li insertion/extraction process in a TiO_2/Li half-cell can be described as follows: $xLi^+ + TiO_2 + xe^- \leftrightarrow Li_xTiO_2$.[11] The theoretical capacity of TiO_2 is 167.5 mAh g^{-1} corresponding to a maximum Li^+ coefficient of 0.5. Figure 7a shows the representative cyclic voltammogram (CV) curves of the anatase TiO_2 NSs at 0.2 mV s^{-1}. In line with previous reports,[14−16] the cathodic peak at ∼1.68 V and anodic peak at ∼2.13 V were observed, corresponding to the reversible transition from tetragonal anatase (I41/amd) to orthorhombic $Li_{0.5}TiO_2$ (*Imma*).[16,33] The voltage profiles at 1 C (170 mA g^{-1}) in Figure 7b exhibit voltage plateaus at ∼1.75 for lithium insertion and ∼2.0 V for lithium extraction, which is consistent with CV curves as well as previously reported data.[14,16,33] The discharge curves reveal that the lithiation process involves three different stages.[16,33,34] The voltage drop from the open-circuit voltage to the onset of the voltage plateau at ca. 1.75 V is attributed to the insertion of a small amount of Li^+ into anatase TiO_2 for formation of solid solution of Li_xTiO_2 and anatase TiO_2.[34] Afterward, Li^+ insert into the interstitial octahedral sites in the anatase TiO_2, entailing a long plateau at 1.75 V.[16,34] In the third stage, the voltage slumped from 1.75 to 1 V, indicating lithiation occurs at the surface layer of the electrode material when the interstitial octahedral sites are occupied.[34] The initial discharge capacity was 192.1 mAh g^{-1} and the subsequent charge capacity was 169.1 mAh g^{-1}, suggesting a 12.5% of irreversible capacity loss, which is much lower than that of other anatase TiO_2 electrodes (30−50%).[35−37] In the second cycle, the discharge and charge capacities were 177.6 mAh g^{-1} and 164.5 mAh g^{-1}, respectively, resulting in an improved Coulumbic efficiency of 92.6%, which was further increased to ∼100% during the following cycles, respectively. The increased Coulombic efficiency reflects that the irreversible loss in capacity arising from Li^+ trapped inside the TiO_2 framework alleviates during cycling.[16,36]

dx.doi.org/10.1021/am504971h | *ACS Appl. Mater. Interfaces* 2014, 6, 19176−19183

The comparative cycling performances of the prepared anatase TiO_2 NSs and commercially available Degussa P25 TiO_2 NPs at different current rates of 1 and 10 *C* are shown in Figure S9 (Supporting Information) and Figure 7c, respectively. At 1 *C*, the anatase TiO_2 NSs delivered a higher discharge capacity of 143.6 mAh g^{-1} than that of the P25 TiO_2 NPs (105.5 mAh g^{-1}) after running for 100 cycles. At higher current rate of 10 *C*, the anatase TiO_2 NSs electrodes still had a reversible capacity of 101.9 mAh g^{-1} after 100 cycles, in stark contrast with P25 TiO_2 NPs (32.3 mAh g^{-1}). Figure 7d presents the comparative rate performance of the anatase TiO_2 NSs and P25 TiO_2 NPs electrodes from 0.5 to 10 *C*. When cycled at 0.5, 1, and 2 *C*, the anatase TiO_2 NSs delivered reversible discharge capacities of 180.2, 164.2, and 145.1 mAh g^{-1} after running for 10 cycles, respectively. Even at 5 and 10 *C*, reversible capacities of 114.3 and 98.8 mAh g^{-1} were still obtained, respectively. The capacity recovered to 135.6 mAh g^{-1} when back to 1 *C*. However, the P25 TiO_2 NPs were susceptible to current rate, as exemplified by a dramatic capacity drop at high rate. At 0.5, 1, 2, 5, and 10 C, their corresponding reversible discharge capacities are 145.4, 120.8, 92.5, 53.7, and 35.3 mAh g^{-1}, respectively. When the rate recovered to 1 *C*, only 98.3 mAh g^{-1} was recorded after 70 cycles at various rates. These results demonstrate the excellent rate performance of the ultrathin anatase TiO_2 NSs with dominated {001} facets. As the measured specific surface areas for P25 TiO_2 NPs and the as-prepared anatase TiO_2 NSs are 51 and 60 m^2 g^{-1}, respectively, the excellent electrochemical performances of the prepared anatase TiO_2 NSs could be mainly attributed to their ultrathin thickness in [001] direction with a large proportion of {001} exposed facets, which allows fast and efficient lithium insertion/extraction.[18]

4. CONCLUSIONS

In summary, anatase TiO_2 NSs with 82% of {001} facets exposed and a 10 nm of thickness were successfully prepared through a facile toluene-water biphasic interfacial reaction method. Furthermore, these prepared ultrathin anatase TiO_2 NSs have clean {001} active facets. This method could enrich the synthesis methods for ultrathin anatase TiO_2 NSs with high-energy {001} facets. It was revealed that anatase TiO_2 NSs could only be prepared through the two-phase interface reaction at high HCl concentration and the reaction time was no less than 5 fours. The prepared anatase TiO_2 NSs exhibited remarkable capability in lithium storage, as verified by a low initial irreversible capacity loss as well as decent capacity retention at high rate up to 10 *C*. Apart from applications in high-power lithium ion batteries, these anatase TiO_2 NSs would be also of great interest for photocatalysis and dye-sensitized solar cells.

■ ASSOCIATED CONTENT

Ⓢ Supporting Information

Statistical data for the side length and thickness of the anatase TiO_2 NSs. FESEM images and XRD pattern of the products prepared with hexane and cyclohexane as organic phases. Side-view TEM image of a single TiO_2 nanosheet and geometric model of the prepared anatase TiO_2 NSs. FESEM image and XRD patterns of the product obtained by using H_2SO_4 instead of HCl. XRD pattern of the products synthesized at different reaction times. XPS spectra of the prepared anatase TiO_2 NSs. Cycling performances of anatase TiO_2 NSs and commercial P25 TiO_2 NPs at 1 C. This material is available free of charge via the Internet at http://pubs.acs.org.

■ AUTHOR INFORMATION

Corresponding Author

*E-mail: jsjiang@phy.ecnu.edu.cn. Tel: +86-21-54342940.

Notes

The authors declare no competing financial interest.

■ ACKNOWLEDGMENTS

This work was supported by the National Natural Science Foundation of China (Grant 21173084) and Large Instruments Open Foundation of East China Normal University. The authors appreciate Prof. Li-Kun Pan for his help in preparation of coin-type cells.

■ REFERENCES

(1) Kamat, P. V. TiO_2 Nanostructures: Recent Physical Chemistry Advances. *J. Phys. Chem. C* **2012**, *116*, 11849−11851.

(2) Oveisi, H.; Rahighi, S.; Jiang, X. F.; Nemoto, Y.; Beitollahi, A.; Wakatsuki, S.; Yamauchi, Y. Unusual Antibacterial Property of Mesoporous Titania Films: Drastic Improvement by Controlling Surface Area and Crystallinity. *Chem. Asian J.* **2010**, *5*, 1978−1983.

(3) Yamauchi, Y. Field-Induced Alignment Controls of One-dimensional Mesochannels in Mesoporous Materials. *J. Ceram. Soc. Jpn.* **2013**, *121*, 831−840.

(4) Weng, W.; Higuchi, T.; Suzuki, M.; Fukuoka, T.; Shimomura, T.; Ono, M.; Radhakrishnan, L.; Wang, H.; Suzuki, N.; Oveisi, H.; Yamauchi, Y. A High-Speed Passive-Matrix Electrochromic Display Using a Mesoporous TiO_2 Electrode with Vertical Porosity. *Angew. Chem., Int. Ed.* **2010**, *49*, 3956−3959.

(5) Wu, K. C. W.; Jiang, X. F.; Yamauchi, Y. New Trend on Mesoporous Films: Precise Controls of One-dimensional (1D) Mesochannels Toward Innovative Applications. *J. Mater. Chem.* **2011**, *21*, 8934−8939.

(6) Liu, S.; Yu, J.; Jaroniec, M. Anatase TiO_2 with Dominant High-Energy {001} Facets: Synthesis, Properties, and Applications. *Chem. Mater.* **2011**, *23*, 4085−4093.

(7) Fang, W. Q.; Gong, X. Q.; Yang, H. G. On the Unusual Properties of Anatase TiO_2 Exposed by Highly Reactive Facets. *J. Phys. Chem. Lett.* **2011**, *2*, 725−734.

(8) Gong, X. Q.; Selloni, A. Reactivity of Anatase TiO_2 Nanoparticles: the Role of the Minority (001) Surface. *J. Phys. Chem. B* **2005**, *109*, 19560−19562.

(9) Han, X.; Kuang, Q.; Jin, M.; Xie, Z.; Zheng, L. Synthesis of Titania Nanosheets with a High Percentage of Exposed (001) Facets and Related Photocatalytic Properties. *J. Am. Chem. Soc.* **2009**, *131*, 3152−3153.

(10) Yang, H. G.; Liu, G.; Qiao, S. Z.; Sun, C. H.; Jin, Y. G.; Smith, S. C.; Zou, J.; Cheng, H. M.; Lu, G. Q. Solvothermal Synthesis and Photoreactivity of Anatase TiO_2 Nanosheets with Dominant {001} Facets. *J. Am. Chem. Soc.* **2009**, *131*, 4078−4083.

(11) Amano, F.; Prieto-Mahaney, O. O.; Terada, Y.; Yasumoto, T.; Shibayama, T.; Ohtani, B. Decahedral Single-Crystalline Particles of Anatase Titanium(IV) Oxide with High Photocatalytic Activity. *Chem. Mater.* **2009**, *21*, 2601−2603.

(12) Yu, J.; Qi, L.; Jaroniec, M. Hydrogen Production by Photocatalytic Water Splitting over Pt/TiO_2 Nanosheets with Exposed (001) Facets. *J. Phys. Chem. C* **2010**, *114*, 13118−13125.

(13) Yu, J.; Fan, J.; Lv, K. Anatase TiO_2 Nanosheets with Exposed (001) Facets: Improved Photoelectric Conversion Efficiency in Dye-Sensitized Solar Cells. *Nanoscale* **2010**, *2*, 2144−2149.

(14) Chen, J. S.; Lou, X. W. Anatase TiO_2 Nanosheet: An Ideal Host Structure for Fast and Efficient Lithium Insertion/Extraction. *Electrochem. Commun.* **2009**, *11*, 2332−2335.

(15) Sun, C. H.; Yang, X. H.; Chen, J. S.; Li, Z.; Lou, X. W.; Li, C.; Smith, S. C.; Lu, G. Q.; Yang, H. G. Higher Charge/Discharge Rates of

Lithium-Ions Across Engineered TiO_2 Surfaces Leads to Enhanced Battery Performance. *Chem. Commun.* **2010**, *46*, 6129−6131.
(16) Chen, J. S.; Tan, Y. L.; Li, C. M.; Cheah, Y. L.; Luan, D.; Madhavi, S.; Boey, F. Y. C.; Archer, L. A.; Lou, X. W. Constructing Hierarchical Spheres from Large Ultrathin Anatase TiO_2 Nanosheets with Nearly 100% Exposed (001) Facets for Fast Reversible Lithium Storage. *J. Am. Chem. Soc.* **2010**, *132*, 6124−6130.
(17) Hengerer, R.; Kavan, L.; Krtil, P.; Grätzel, M. Orientation Dependence of Charge-Transfer Processes on TiO_2 (Anatase) Single Crystals. *J. Electrochem. Soc.* **2000**, *147*, 1467−1472.
(18) Chen, J. S.; Archer, L. A.; Lou, X. W. SnO_2 Hollow Structures and TiO_2 Nanosheets for Lithium-Ion Batteries. *J. Mater. Chem.* **2011**, *21*, 9912−9924.
(19) Liu, G.; Yu, J. C.; Lu, G. Q.; Cheng, H. M. Crystal Facet Engineering of Semiconductor Photocatalysts: Motivations, Advances and Unique Properties. *Chem. Commun.* **2011**, *47*, 6763−6783.
(20) Yang, H. G.; Sun, C. H.; Qiao, S. Z.; Zou, J.; Liu, G.; Smith, S. C.; Cheng, H. M.; Lu, G. Q. Anatase TiO_2 Single Crystals With a Large Percentage of Reactive Facets. *Nature* **2008**, *453*, 638−642.
(21) Liu, G.; Sun, C.; Yang, H. G.; Smith, S. C.; Wang, L.; Lu, G. Q.; Cheng, H. M. Nanosized Anatase TiO_2 Single Crystals for Enhanced Photocatalytic Activity. *Chem. Commun.* **2010**, *46*, 755−757.
(22) Liu, G.; Yang, H. G.; Wang, X. W.; Cheng, L. N.; Pan, J.; Lu, G. Q.; Cheng, H. M. Visible Light Responsive Nitrogen Doped Anatase TiO_2 Sheets with Dominant {001} Facets Derived from TiN. *J. Am. Chem. Soc.* **2009**, *131*, 12868−12869.
(23) Yu, J.; Dai, G.; Xiang, Q.; Jaroniec, M. Fabrication and Enhanced Visible-Light Photocatalytic Activity of Carbon Self-Doped TiO_2 Sheets With Exposed {001} Facets. *J. Mater. Chem.* **2011**, *21*, 1049−1057.
(24) Liu, G.; Yang, H. G.; Wang, X.; Cheng, L.; Lu, H.; Wang, L.; Lu, G. Q.; Cheng, H. M. Enhanced Photoactivity of Oxygen-Deficient Anatase TiO_2 Sheets with Dominant {001} Facets. *J. Phys. Chem. C* **2009**, *113*, 21784−21788.
(25) Wu, B.; Guo, C.; Zheng, N.; Xie, Z.; Stucky, G. D. Nonaqueous Production of Nanostructured Anatase with High-Energy Facets. *J. Am. Chem. Soc.* **2008**, *130*, 17563−17568.
(26) Zhang, D.; Li, G.; Yang, X.; Yu, J. C. A Micrometer-size TiO_2 Single-Crystal Photocatalyst With Remarkable 80% Level of Reactive Facets. *Chem. Commun.* **2009**, 4381−4383.
(27) Zhu, J.; Wang, S.; Bian, Z.; Xie, S.; Cai, C.; Wang, J.; Yang, H.; Li, H. Solvothermally Controllable Synthesis of Anatase TiO_2 Nanocrystals With Dominant {001} Facets and Enhanced Photocatalytic Activity. *CrystEngComm* **2010**, *12*, 2219−2224.
(28) Alivov, Y.; Fan, Z. Y. A Method for Fabrication of Pyramid-Shaped TiO_2 Nanoparticles with a High {001} Facet Percentage. *J. Phys. Chem. C* **2009**, *113*, 12954−12957.
(29) Gordon, T. R.; Cargnello, M.; Paik, T.; Mangolini, F.; Weber, R. T.; Fornasiero, P.; Murray, C. B. Nonaqueous Synthesis of TiO_2 Nanocrystals Using TiF_4 to Engineer Morphology, Oxygen Vacancy Concentration, and Photocatalytic Activity. *J. Am. Chem. Soc.* **2012**, *134*, 6751−6761.
(30) Yang, X. H.; Li, Z.; Sun, C.; Yang, H. G.; Li, C. Hydrothermal Stability of {001} Faceted Anatase TiO_2. *Chem. Mater.* **2011**, *23*, 3486−3494.
(31) Wu, L.; Yang, B. X.; Yang, X. H.; Chen, Z. G.; Li, Z.; Zhao, H. J.; Gong, X. Q.; Yang, H. G. On The Synergistic Effect of Hydrohalic Acids In The Shape-Controlled Synthesis of Anatase TiO_2 Single Crystals. *CrystEngComm* **2013**, *15*, 3252−3255.
(32) Zhao, Z.; Sun, Z.; Zhao, H.; Zheng, M.; Du, P.; Zhao, J.; Fan, H. Phase Control of Hierarchically Structured Mesoporous Anatase TiO_2 Microspheres Covered With {001} Facets. *J. Mater. Chem.* **2012**, *22*, 21965−21971.
(33) Ma, Y.; Ji, G.; Ding, B.; Lee, J. Y. Facile Solvothermal Synthesis of Anatase TiO_2 Microspheres with Adjustable Mesoporosity For The Reversible Storage of Lithium Ions. *J. Mater. Chem.* **2012**, *22*, 24380−24385.
(34) Jiang, C.; Wei, M.; Qi, Z.; Kudo, T.; Honma, I.; Zhou, H. Particle Size Dependence of The Lithium Storage Capability and High Rate Performance of Nanocrystalline Anatase TiO_2 Electrode. *J. Power Sources* **2007**, *166*, 239−243.
(35) Ding, S.; Chen, J. S.; Wang, Z.; Cheah, Y. L.; Madhavi, S.; Hu, X.; Lou, X. W. TiO_2 Hollow Spheres with Large Amount of Exposed (001) Facets for Fast Reversible Lithium Storage. *J. Mater. Chem.* **2011**, *21*, 1677−1680.
(36) Song, B.; Liu, S. W.; Jian, J. K.; Lei, M.; Wang, X. J.; Li, H.; Yu, J. G.; Chen, X. L. Electrochemical Properties of TiO_2 Hollow Microspheres From a Template-Free and Green Wet-Chemical Route. *J. Power Sources* **2008**, *180*, 869−874.
(37) Wang, Z.; Lou, X. W. TiO_2 Nanocages: Fast Synthesis, Interior Functionalization and Improved Lithium Storage Properties. *Adv. Mater.* **2012**, *24*, 4124−4129.